



**HAL**  
open science

## Numerical simulation of the thermoforming of multi-layer polymer sheets

Marie-Hélène Vantal, Bernard Monasse, Michel Bellet

► **To cite this version:**

Marie-Hélène Vantal, Bernard Monasse, Michel Bellet. Numerical simulation of the thermoforming of multi-layer polymer sheets. Proceedings NUMIFORM'95, 5th Int. Conf. on Numerical Methods in Industrial Forming Processes, Jun 1995, Ithaca, NY, United States. pp.Pages 1089-1095. hal-00576335

**HAL Id: hal-00576335**

**<https://minesparis-psl.hal.science/hal-00576335>**

Submitted on 14 Mar 2011

**HAL** is a multi-disciplinary open access archive for the deposit and dissemination of scientific research documents, whether they are published or not. The documents may come from teaching and research institutions in France or abroad, or from public or private research centers.

L'archive ouverte pluridisciplinaire **HAL**, est destinée au dépôt et à la diffusion de documents scientifiques de niveau recherche, publiés ou non, émanant des établissements d'enseignement et de recherche français ou étrangers, des laboratoires publics ou privés.

# Numerical simulation of the thermoforming of multi-layer polymer sheets

Marie-Hélène Vantal, Bernard Monasse, Michel Bellet

*Ecole des Mines de Paris, CEMEF, Centre de Mise en Forme des Matériaux, UA CNRS 1374, Sophia Antipolis, France*

Proc. NUMIFORM'95, 5th Int. Conf. on Numerical Methods in Industrial Forming Processes, Cornell University, Ithaca (NY, USA), June 18-21 1995, S.-F. Shen & P.R. Dawson (eds.), Balkema, Rotterdam, pp.1089-1095 (1995)

**ABSTRACT:** This paper presents a 3D finite element model of the thermoforming process. The polymer material is assumed to obey the viscoplastic law proposed by G'Sell and Jonas, the coefficient of which have been identified for a polystyrene. The implementation of this constitutive model, the heat transfer coupling and the proposed multi-layer approach are detailed in the paper. Axisymmetric validation tests and an application to the thermoforming of an industrial component are also reported.

## 1 INTRODUCTION

The thermoforming process consists in heating a polymer sheet and shaping it inside a mold. The deformation results from a pressure cycle eventually coupled with the use of a moving tool. The forming of thin products made of various polymer materials is carried out by this method: rubbery amorphous, solid semi-crystalline or multi-layer composites. The heating temperature depends upon the selected polymer. At low temperature, the forming is limited by the too high rigidity of the sheet. On the contrary, at high temperature, the sheet deforms by gravity and the forming is very difficult to control. Hence, the thermoforming is operated above the glass transition temperature ( $T_g$ ), in the rubber-like behavior domain for amorphous polymers, and close to the melting temperature for semi-crystalline polymers.

The main problem of the process is the thinning in the corners of the parts, which leads to a decrease of the mechanical properties of the shaped components. The optimization of the final thickness profile is generally achieved by trial-and-error, changing the design of the component, the polymer material, and the process parameters such as the heating temperature distribution, the mold temperature, the pressure curve, or using a punch for deep parts. The numerical modelling should then result in a more efficient optimization of the process.

Various numerical simulation models have been proposed (Warby & Whiteman 1988, De Lorenzi & Nied 1991, Kouba et al. 1992, Shrivastava & Tang 1993). Regarding the application to three-dimensional formings, they are generally based on the membrane mechanical approximation, associated with the finite element method. Those computations use either hyperelastic (De Lorenzi & Nied 1991, Shrivastava & Tang 1993) or viscoelastic (Warby &

Whiteman 1988, Kouba et al. 1992) constitutive equations, without any heat transfer coupling and a sticking contact hypothesis at polymer-tools interface.

It should be pointed out that this latter assumption has no experimental evidence. Most of the time, it is used just because the computation is isothermal and cannot account for the decrease of the polymer temperature and its "freezing" after tool contact. Another thermomechanical coupling is the high self heating source term due to the high strain rates. As the behavior of polymers is known to be highly temperature-dependent, it seems essential to couple heat transfer and mechanical models.

In the present paper, we describe a 3D finite element model with membrane approximation to predict the deformation. Concerning the contact conditions with punch and mold, either sliding contact with Coulomb's friction law or sticking contact can be considered. The paper is focused on the thermal evolution effects during the forming, and on the approach to multilayer sheet forming.

## 2 MATERIAL BEHAVIOR IDENTIFICATION

The one-dimensional constitutive equation initially proposed by G'Sell and Jonas (1979) has been selected in the context of polymer thermoforming:

$$\bar{\sigma} = K_p(T) [1 - \exp(-w\bar{\epsilon})] \exp(h\bar{\epsilon}^2) \bar{\epsilon}^m \quad (1)$$

where  $T$  is the temperature,  $\bar{\epsilon}$  the von Mises equivalent strain-rate,  $\bar{\epsilon}$  the von Mises equivalent strain.  $K_p$ ,  $w$ ,  $h$  and  $m$  are material parameters.

This law accounts for the material behavior of a great number of polymers, either amorphous or semi-crystalline, in a large temperature interval. Duffo et al. (1994) have identified parameters for

polypropylene by means of tensile tests on sheets, yielding:

$$K_p = 5.31 \cdot 10^{-3} \exp [2.85 \cdot 10^{-3} / T] \text{ MPa}\cdot\text{s}^m$$

$$w = 20, h = 0.4, m = 0.087$$

We have studied the material behavior of a polystyrene compound, by uniaxial tensile testing at constant axial strain rate. Tests have been carried out at four constant temperatures: 110, 120, 130 and 140°C (which cover the forming temperature domain of this polymer) and five different strain-rates between  $10^{-4}$  and  $10^{-2} \text{ s}^{-1}$ . The associated determination of the coefficients of equation (1) shows the transition from a solid-like behavior to a liquid-like one: see figure 1. The consistency  $K_p$  of the material decreases suddenly above  $T_g$  and keeps low values ( $\approx 2$ ) in the experimental domain. The so-called viscoelastic coefficient  $w$  is found low ( $\approx 3.7$ ) and independent on temperature. Finally, it has appeared that the basic equation (1) has to be modified, in order to include a temperature dependency of the strain-rate sensitivity coefficient  $m$  and the hardening coefficient  $h$ .

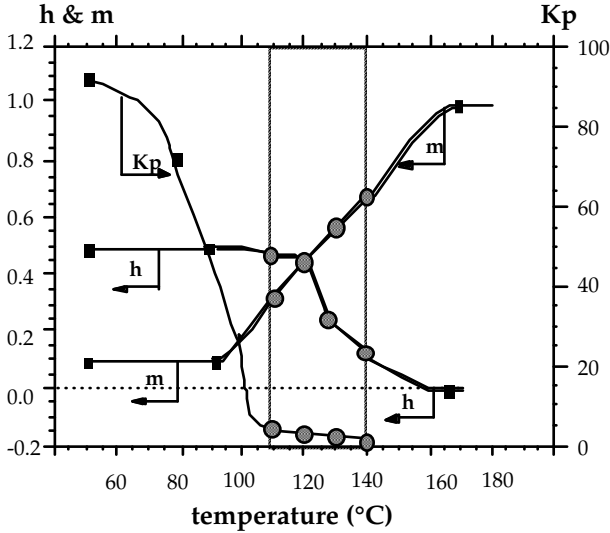


Fig.1 - Coefficients  $m$ ,  $h$  and  $K_p$ (MPa.s<sup>m</sup>) of equ. (1) for polystyrene vs temperature. (Grey dots identified by tensile tests, black squares issued from literature).

### 3 MECHANICAL FORMULATION

#### 3.1 Membrane equilibrium

According to membrane mechanical assumption, the deformed sheet is considered as a geometric surface, neglecting flexion and transverse shear. A material point is identified by two curvilinear coordinates:  $\theta^1$  and  $\theta^2$  which are, in the case of an initial sheet in  $xy$  plane, the initial  $x$  and  $y$  coordinate respectively. At any point of the deformed sheet (vector  $\mathbf{x}$ ) the local tangent basis is defined by:

$$\mathbf{g}_1 = \frac{\mathbf{Zx}}{\check{\theta}^1}, \quad \mathbf{g}_2 = \frac{\mathbf{Zx}}{\check{\theta}^2}, \quad \mathbf{g}_3 = \frac{1}{\|\mathbf{g}_1 \wedge \mathbf{g}_2\|} \mathbf{g}_1 \wedge \mathbf{g}_2 \quad (2)$$

The equilibrium of the deformed sheet is expressed by the principle of virtual work (without inertia):

$$\forall \mathbf{v}^* \int_{\Omega} \boldsymbol{\sigma}^{ij} v_{ij}^* e dS - \int_{\Omega_p} P \mathbf{g}_3 \cdot \mathbf{v}^* dS - \int_{\Omega_c} \mathbf{t} \cdot \mathbf{v}^* dS = 0 \quad (3)$$

where  $\boldsymbol{\sigma}^{ij}$  are the covariant components of the Cauchy stress tensor (plane stress:  $i,j=1,2$ ),  $\cdot_{,ij}$  denotes covariant derivation with respect to  $\theta^j$ ,  $e$  is the sheet thickness,  $\mathbf{t}$  are the friction stresses on regions  $\Omega_c$  contacting the mold,  $P$  is the inflation pressure applied to the domain  $\Omega_p$  of the deformed surface  $\Omega$ .

#### 3.2 Time discretization. Incremental procedure

Starting with a balanced configuration  $\Omega$  at time  $t$ , the problem consists in determining the unknown equilibrated configuration  $\Omega'$  at  $t+\Delta t$ . Variables at  $t+\Delta t$  are denoted "prime". By application of eq.(3) at  $t+\Delta t$ , we have, for any velocity field  $\mathbf{v}^*$ :

$$\int_{\Omega'} \boldsymbol{\sigma}'^{ij} v_{ij}^* e' dS - \int_{\Omega'_p} P' \mathbf{g}'_3 \cdot \mathbf{v}^* dS - \int_{\Omega'_c} \mathbf{t}' \cdot \mathbf{v}^* dS = 0 \quad (4)$$

This equation is solved for the incremental displacement field  $\mathbf{u}$  between  $\Omega$  and  $\Omega'$ , provided that  $\mathbf{t}'$ ,  $e'$  and  $\boldsymbol{\sigma}'$  can be calculated from  $\mathbf{u}$ . Those relations are exposed hereunder and the resolution in 3.3.

- *Contact and friction*: as regard the contact condition applied to  $\Omega_c$ , it may be either sticking (no relative velocity with respect to the mold) or sliding: in this case, the tangential stress is supposed to be given by the Coulomb's friction law (coefficient  $\mu$ ), in which the normal stress is the inflation pressure:

$$\mathbf{t}' = -\mu P' (1 / \|\mathbf{u}\|) \mathbf{u} \quad (5)$$

- *Thickness updating*: the new local thickness  $e'$  is deduced from material incompressibility. Denoting  $\mathbf{g}$  the metric tensor ( $g_{ij} = \mathbf{g}_i \cdot \mathbf{g}_j$ ), we have:

$$e' = e \sqrt{\det(\mathbf{g}) / \det(\mathbf{g}')} \quad (6)$$

- *Resolution of incremental constitutive equations*: the one-dimensional constitutive equation (1) can be written as a classical viscoplastic power law:

$$\bar{\boldsymbol{\sigma}} = k \bar{\boldsymbol{\varepsilon}}^m \quad (7)$$

Hence, the flow rule derives from a viscoplastic potential  $Q$ . Under isotropy assumption, it yields:

$$\dot{\boldsymbol{\varepsilon}} = \frac{\check{\mathbf{Z}}Q}{\check{\mathbf{Z}}\boldsymbol{\sigma}} = \frac{\check{\mathbf{Z}}Q}{\check{\mathbf{Z}}\boldsymbol{\sigma}} \frac{\check{\mathbf{Z}}\boldsymbol{\sigma}}{\check{\mathbf{Z}}\boldsymbol{\sigma}} = \dot{\boldsymbol{\varepsilon}} \frac{\check{\mathbf{Z}}\boldsymbol{\sigma}}{\check{\mathbf{Z}}\boldsymbol{\sigma}} \quad (8)$$

In convective curvilinear coordinates, we have:

$$\dot{\boldsymbol{\varepsilon}}^2 = 2/3 \dot{\boldsymbol{\varepsilon}}^{ij} \dot{\boldsymbol{\varepsilon}}_{ij}, \quad \bar{\boldsymbol{\sigma}}^2 = 3/2 s_{ij} s_{ij} = \boldsymbol{\sigma}^T \mathbf{A} \boldsymbol{\sigma} \quad (9)$$

$$A_{ijkl} = 3/2 g_{ik} g_{jl} - 1/2 g_{ij} g_{kl} \quad (10)$$

The constitutive equation can then be written:

$$\dot{\boldsymbol{\epsilon}} = (\dot{\bar{\boldsymbol{\epsilon}}}) \mathbf{A} \boldsymbol{\sigma} = (1/k) \dot{\bar{\boldsymbol{\epsilon}}}^{(1-m)} \mathbf{A} \boldsymbol{\sigma} \quad (11)$$

A semi-implicit time integration scheme is used over the increment. The incremental strain tensor  $\Delta \boldsymbol{\epsilon}$ , the covariant components of which depend on the displacement  $\mathbf{u}$  according to (12) is written as (13):

$$\Delta \epsilon_{ij} = 1/2 (u_{i|j} + u_{j|i} + u_{m|i} u_{j|}^m) \quad (12)$$

$$\Delta \boldsymbol{\epsilon} = \Delta t [(1-\eta) \dot{\boldsymbol{\epsilon}} + \eta \boldsymbol{\epsilon}'] \quad (13)$$

Equations (11-13) clearly permit to deduce the new local stress tensor  $\boldsymbol{\sigma}'$ , knowing the displacement field  $\mathbf{u}$ . Practically, a fully implicit scheme ( $\eta=1$ ) is used.

### 3.3 Resolution: finite element method (f.e. m.)

Finally, injection of (5-6) and (11-13) in the equilibrium equation (4) leads to a non-linear equation for the displacement field  $\mathbf{u}$ . Its spatial discretization by f.e.m. (linear triangles or quadrangles) is detailed by Bellet (1988, 1990). At every time step a non-linear system for the vector  $\mathbf{U}$  of the nodal displacements is solved by the Newton-Raphson method, with a consistent tangent matrix.

## 4 HEAT TRANSFER RESOLUTION

Considering the thinness of polymer sheets, the short processing times, and the low diffusivity of polymers, it can be assumed that heat transfer is essentially one dimensional across the thickness of the sheet (Vantal 1995). Consequently,  $s$  being the coordinate in the thickness direction ( $s=\theta^3$ ), the 1D heat transfer equation can be expressed:

$$\rho c \frac{dT}{dt} = \frac{\dot{Z}}{\dot{Z}_s} \left( \lambda \frac{\dot{Z}T}{\dot{Z}_s} \right) + \boldsymbol{\sigma} : \dot{\boldsymbol{\epsilon}} \quad (14)$$

where  $\rho$  is the specific mass,  $c$  the heat capacity and  $\lambda$  the heat conductivity. The following boundary conditions are accounted for. At sheet/air interface:

$$-\lambda \frac{\dot{Z}T}{\dot{Z}_s} \text{sgn}(\mathbf{n}) = h_{\text{conv}} (T - T_{\text{air}}) \quad (15)$$

where  $h_{\text{conv}}$  is the coefficient for heat exchange by convection,  $T_{\text{air}}$  the air temperature and  $\text{sgn}(\mathbf{n})$  is  $\pm 1$  depending on the orientation of the outward normal unit vector  $\mathbf{n}$ . At sheet/tool interface, due to the much higher diffusivity of metals, we will assume that the surface temperature of the polymer sheet is prescribed to the interface temperature given by:

$$T_{\text{inter}} = (b_{\text{tool}} T_{\text{tool}} + b_{\text{sheet}} \bar{T}_{\text{sheet}}) / (b_{\text{tool}} + b_{\text{sheet}}) \quad (16)$$

where  $b$  is the thermal effusivity  $\sqrt{\lambda \rho c}$  and  $\bar{T}_{\text{sheet}}$  is the average temperature of the sheet in the thickness. The initial temperature profile is assumed to be known at the beginning of the process.

Equation (14) is discretized in space and time, at each integration point of membrane finite elements,

using a Galerkin 1D f.e.m. (figure 2) and a semi-implicit time integration scheme (Vantal 1995).

The coupling between the mechanical and the thermal resolution is carried out at each time increment as explained in figure 3.

## 5 MULTI-LAYER FORMULATION

The multi-layer approach proposed here is based on the following assumptions:

- each layer is submitted to the same deformation as the mean surface of the sheet. This is consistent with

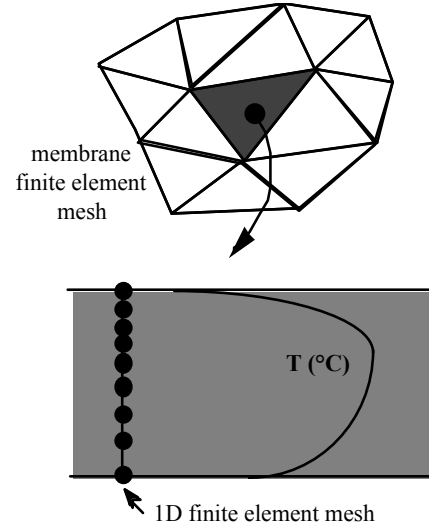


Fig.2 - 1D approach for thermal coupling

A/ Thermal resolution

- for all membrane elements
  - for all integration points of the element
    - perform a 1D f.e. computation of the new temperature profile  $T'$  across the thickness. The source term is given by the mechanical resolution of previous time step.
    - for all integration points  $ipth$  of 1D mesh update the temperature-dependent coefficients:  $K'_p(T')$ ,  $m'(T')$  and  $h'(T')$ .

B/ Mechanical resolution

B1) computation of the residual vector  $\mathbf{R}(U)$

- for all membrane elements
  - for all integration points of the element
    - for all integration points  $ipth$  of 1D mesh solve the constitutive equations for  $\sigma'(ipth)$  and  $\partial\sigma'/\partial\Delta\epsilon(ipth)$ , using the updated values of material coefficients:  $K'_p(ipth)$ ,  $m'(ipth)$  and  $h'(ipth)$
    - compute thickness-averaged values  $\langle\sigma'\rangle$  and  $\langle\partial\sigma'/\partial\Delta\epsilon\rangle$  and sum in residual vector.

B2) iterative Newton-Raphson procedure to solve  $\mathbf{R}(U)=0$

Fig.3 - Thermo-mechanical coupling algorithm.

the membrane approach in which transverse shear and flexion are neglected. Hence, the thickness ratio of the different layers remains constant during the process.

- accordingly, the mechanical and thermal contact are assumed perfect (no sliding, no thermal contact resistance) at interfaces between layers.

The algorithm is identical to the one for heat transfer coupling, except that all thermal and mechanical parameters used at integration points in thickness ( $ipth$ ) will now depend upon the material in which they are located (see fig. 4). Each layer material has an identified temperature dependent behavior law.

Such a formulation is expected to be more precise than the reduction of the multi-layer to a single "equivalent" material, especially when steep temperature gradients appear in the sheet thickness when one side of the multi-layer contacts the tooling.

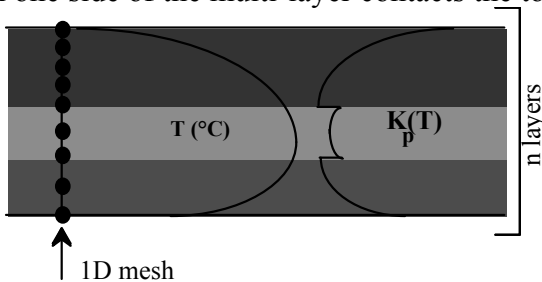


Fig.4 - Multi-layer formulation (schematic).

6.1 Experimental: axisymmetric thermoforming test

Formings were carried out on a small machine equipped with contact sensors and pressure gauges.

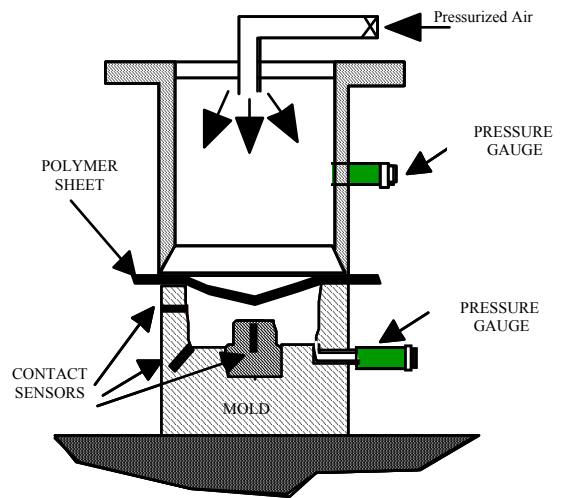


Fig. 5 - Experimental thermoforming system (the optional punch system is not shown here).

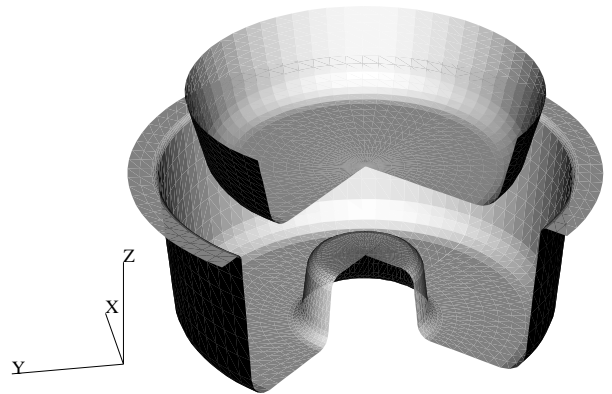


Fig. 6 - Mold and punch view.

The mold geometry is axisymmetric (diameter  $\approx$  140 mm, depth 60 mm), including a central insert in the bottom (see fig. 6) which makes it very sensitive both to cooling and friction effects. The forming parameters are the followings: aluminium mold, 20°C, air temperature = 20°C, linear pressure vs time: 0.6 MPa.s<sup>-1</sup>, initial sheet temperature 130°C. The one-layer polystyrene sheet is initially 1.1 mm thick. Its orientation due to extrusion is relatively high, and it involves an evolution of the thickness during infrared heating as it is clamped. Consequently, the measured final thickness profile depends upon the measurement direction (extrusion or transverse direction, see fig.7).

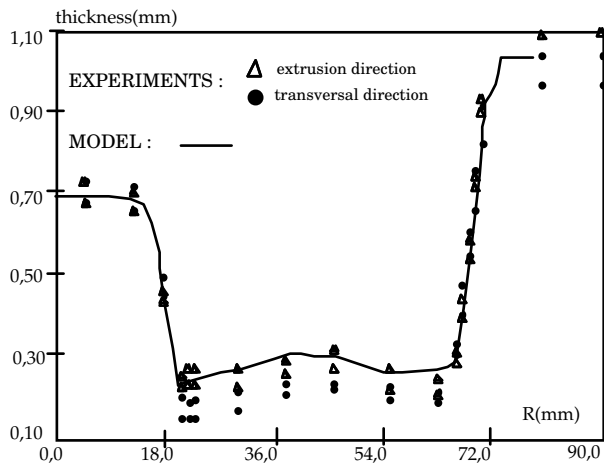


Fig. 7 - Comparison between measured and computed thickness distribution.

### 6.2 Numerical simulation of the test

Due to axisymmetry, only a narrow sector has been meshed with 160 triangles. We have used the rheological data of fig.1 and the following values of thermal parameters:  $\rho c = 1.92 \cdot 10^6 \text{ J.m}^{-3}.\text{K}^{-1}$ ,  $\lambda = .2 \text{ W.m}^{-1}.\text{K}^{-1}$ ,  $h = 33 \text{ W.m}^{-2}.\text{K}^{-1}$ . A Coulomb friction has been accounted for ( $\mu=0.4$ ).

The predicted final thickness profile, using the coupled thermomechanical model, is in good agreement with the measurements (figure 7).

Regarding kinematics, it should be noticed that the measured differential pressure was found very low. The use of these values as a prescribed boundary condition ( $P(t)$  in equation (3)) has lead to much slower forming rates than the actual ones. However, if the measured upper pressure is used instead of the differential pressure, then computed forming times are in agreement with experimental ones, as shown in table 1. This unexpected result needs more investigation.

contact time (s) at sensor #	1	2	3
experiment	0.095 s	0.400 s	0.510 s
computation	0.102 s	0.311 s	0.390 s

Table 1

### 6.3 Influence of thermal coupling

On figure 8, three different computed thickness profiles have been plotted, using three different computational options.

As already said, the assumption of sticking contact has no clear experimental evidence. However, as shown on figure 8, it is the only means to get reasonable results if an isothermal model is used. For example the combination (isothermal ; high friction) yields completely erroneous thicknesses (far too low on the insert, despite the high friction coefficient)!

On another hand, the use of the present non-isothermal formulation permits to decouple clearly the frictional and the thermal effects: the quick cooling of the polymer when contacting the mold increases the consistency and the hardening

coefficient of the material for the contact zones, as the strain-rate sensitivity coefficient decreases. The evolution of these coefficients localize the deformation in the warmer zones: the strain-rate values are almost zero in the "frozen" zones. The non-isothermal model is much more representative of the local phenomena in thermoforming and is able to account independently for interface tribology and heat transfer.

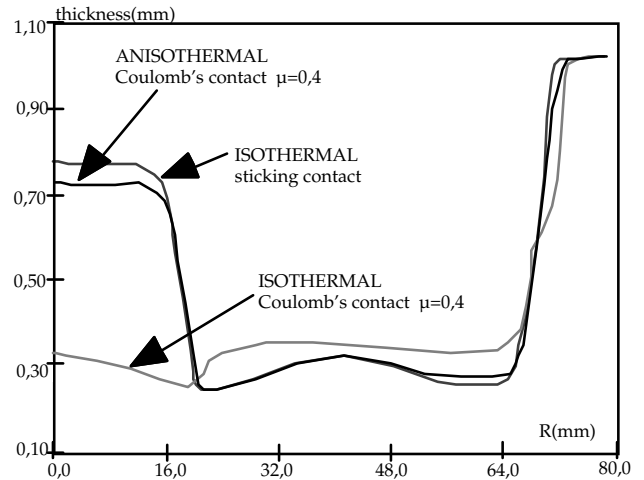


Fig.8 - Computed thickness for three models.

### 6.4 Multi-layer application

We have simulated the forming of a bi-layer: 80% polystyrene (PS), 20% polypropylene (PP), total thickness 1mm. The rheological parameters for both polymers are those given in section 2. The sheet is formed successively with a punch ( $z=-30\text{mm}$  at 0.15 s) and pressure (linear increase of 0.8 MPa between 0.15 s and 0.65 s). The initial temperatures are  $20^\circ\text{C}$  for tools and  $150^\circ\text{C}$  for the sheet.

It is shown in table 2 and figure 9 that the deformation of the bilayer is not a simple addition or average of the deformation of each layer component

PP only	PP_PS PP on top	PS_PP PS on top	PS only
0.59 s	0.50 s	0.39 s	0.45 s

Table 2 - Predicted forming times.

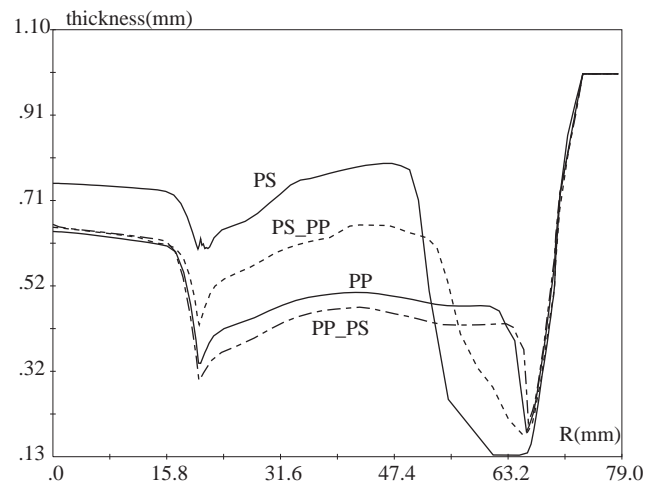


Fig.9 - Computed thickness profiles.

with the same thickness. In addition, the results clearly depend on which material is on top.

This is due to the fact that the cooling effect is different for PS or PP: the consistency of PS decreases suddenly above  $T_g$  whereas it follows an Arrhenius law for PP. Also  $m$  and  $h$  are temperature dependent for PS whereas constant for PP.

## 7 APPLICATION: INDUSTRIAL FORMING

In order to test the robustness and the results of the code, the forming of a one-layer shallow component for food packaging has been studied (fig. 10).

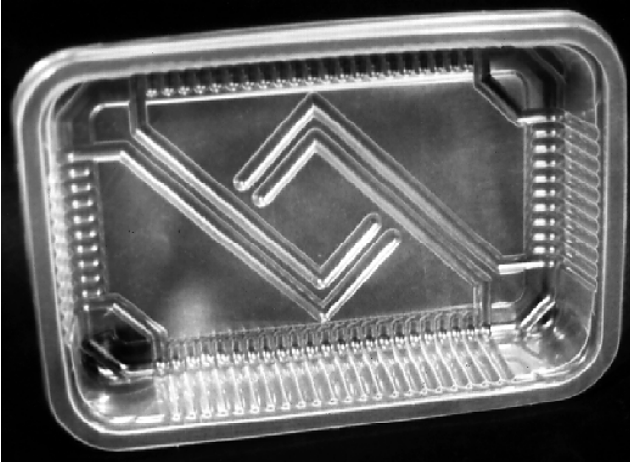


Fig.10 - Selected polypropylene test part.

The material is polypropylene, initially 0.475 mm thick. The industrial forming conditions have not been accurately measured, but the following figures can be considered realistic: aluminum mold ( $5^\circ\text{C}$ ), linear pressure reaching 0.7MPa at 0.5s, air temperature  $20^\circ\text{C}$ , initial sheet temperature  $150^\circ\text{C}$ .

Only a quarter of the symmetrized actual forming has been computed, using 7591 and 6463 triangles for the sheet and mold meshes respectively. A Coulomb's friction law ( $\mu=0.4$ ) is assumed at the mold surface, except near the edge where sticking contact is prescribed. As shown on fig. 12, the central bulging of the sheet is very fast, reaching the bottom at 0.04s. The forming is then slowed down until the end.

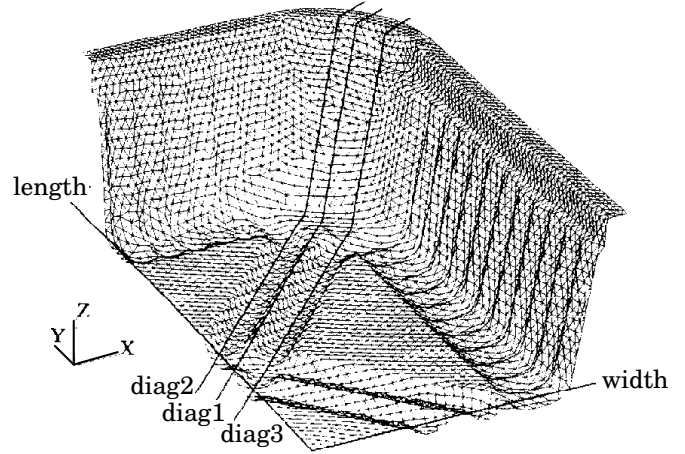


Fig.11 - Final deformed finite element mesh and selected directions for thickness comparison.

experimental dispersion has been found high (up to 18% of the

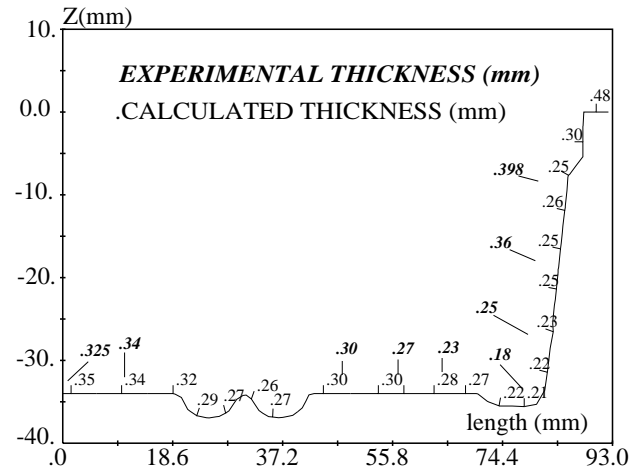


Fig. 13 - Example of comparison between measured and computed thickness ("length" on figure 12).

average value). The average of relative errors between computed and average experimental thickness is good: 10% at the bottom, 18% at wall.

## 8 CONCLUSION

Thermomechanical coupling and a multi-layer approach have been implemented in a finite element membrane model. They are shown to be very efficient tools to improve the predictive character of finite element simulations of thermoforming.

## 9 ACKNOWLEDGEMENT

The experimental part of this work has been done at Elf-Atochem (Cerdato) which has also supported this study.

## 10 REFERENCES

- Bellet M. 1988. Modélisation numérique du formage superplastique de tôles. Doctorate thesis (in french), Ecole des Mines de Paris.
- Bellet M., Massoni E. and Chenot J.L. 1990. Numerical simulation of thin sheet forming processes by the finite element method. *Eng. Comp.*, 7, p. 21.
- De Lorenzi H.G. & Nied H.F. 1991. Finite element simulation of thermoforming and blow molding. *Modelling of Polymer Processing*, A.I.Isayev (ed.), Hanser Verlag, chap.5, pp. 118-171.
- Duffo P., Monasse B., Haudin J.M., G'Sell C. & Dahoun A. 1994. Rheology of polypropylene in the solid state. *J. Mater. Sci.*, 29.
- G'Sell C. & Jonas J.J. 1979. Determination of the plastic behavior of solid polymers at constant true strain rate. *J. Mat. Sci.*, 14, pp. 583-591.
- Kouba K., Bartos O. & Vlachopoulos J. 1992. Computer simulation of thermoforming in complex shapes. *Polym. Eng. Sci.*, 32, pp. 699-704.
- Shrivastava S. & Tang J. 1993. Large deformation finite element analysis of viscoelastic membranes with reference to thermoforming. *J. Strain Anal.*, 28, pp. 21-51.
- Vantal M-H. 1995. Etude numérique et expérimentale du thermoformage des polymères". Doctorate thesis (in french), Ecole des Mines de Paris.

Fig. 12 - Computed deformed sheet

Figure 11 shows the deformed finite element mesh at the end of the process. Iso-values of temperature (not shown here) indicate that during forming the free regions are the warmer (close to the initial temperature), and that in contacting regions, the longer the contact duration, the cooler is the sheet.

The final thickness of actual parts has been measured along the five directions mentioned on figure 11. An example of comparison with the computed values is shown in figure 13. Experimental points are issued from measurements on two different parts, yielding four values per point. The

Warby M.K. & Whiteman J.R. 1988. Finite element model of viscoelastic membrane deformation. *Comput. Struct.*, 68, pp. 33-54.